# Anisotropic Photoinduced Magnetism in Thin Films of the Prussian Blue Analogue $A_jCo_k[Fe(CN)_6]_l \cdot nH_2O$

Franz A. Frye,[‡,†] Daniel M. Pajerowski,[§] Ju-Hyun Park,[⊥,§] Mark W. Meisel,*[,§] and Daniel R. Talham*[,†]

*Department of Chemistry, University of Florida, Gainesville, Florida 32611-7200, and Department of Physics, Center for Condensed Matter Sciences, University of Florida, Gainesville, Florida 32611-8440*

*Received February 27, 2008. Revised Manuscript Received June 10, 2008*

The photoinduced magnetism in thin films of the Prussian blue analogue $A_jCo_k[Fe(CN)_6]_l \cdot nH_2O$ deposited on Melinex solid supports is anisotropic, exhibiting a photoinduced increase when oriented parallel to the external magnetic field and a decrease when oriented perpendicular. The anisotropic behavior is observed for films less than ~200 nm thick below nominally 10 K, which is less than the ferrimagnetic ordering temperature ($T_C$) of 17 K, and in applied fields of less than ~1.5 kG. The thin films with formulas $Rb_{0.7}Co_4[Fe(CN)_6]_{3.0}$, $Rb_{2.3}Co_4[Fe(CN)_6]_{3.1}$, and $K_{0.5}Co_4[Fe(CN)_6]_{3.2}$ were generated using sequential adsorption methods, alternately immersing the Melinex solid support in solutions of the constituent $Co^{2+}$ and $[Fe(CN)_6]^{3-}$ ions. Film thickness is controlled by the number of deposition cycles and by variations in the deposition protocols. Measurements on films with different alkali ions and with different stoichiometry indicate that the microscopic mechanism for the photoinduced magnetization is the same in the films as in the bulk material. The unique anisotropy is qualitatively associated with the interface between the magnetic film and the solid support. Detailed studies of the influence of film thickness, applied field strength, and temperature support this description.

## Introduction

Photoinduced magnetism in the cobalt iron Prussian blue analogue $A_jCo_k[Fe(CN)_6]_l \cdot nH_2O$ was reported by Hashimoto and co-workers in 1996[1] and subsequently studied by several groups.[2–14] Diamagnetic $Co^{III}$(ls)−$Fe^{II}$ pairs may be photoexcited to a long-lived metastable ferrimagnetic $Co^{II}$(hs)−$Fe^{III}$ state through a charge transfer and spin-crossover event increasing the magnetization. Although still a low-temperature phenomenon, many potential applications of this exciting class of material will require fabrication of thin films. We undertook a study of the $A_jCo_k[Fe(CN)_6]_l \cdot nH_2O$ system as part of our program[15–23] to develop fabrication methods for thin films of molecule-based magnetic materials. Investigation of the magnetic and photomagnetic properties of $A_jCo_k[Fe(CN)_6]_l \cdot nH_2O$ showed that in addition to the magnetic and photomagnetic phenomena present in powdered solids, the thin films exhibit a new phenomenon, a photoinduced decrease in magnetization for a specific orientation of the film in the applied magnetic field.[20] The photomagnetic response of the thin films is anisotropic, increasing in one

* To whom correspondence should be addressed. E-mail: talham@chem.ufl.edu (D.R.T.) or meisel@phys.ufl.edu (M.W.M.).
† Department of Chemistry, University of Florida.
‡ Present address: Department of Physical Sciences, Concord University, Athens, WV 24712-1000.
§ Department of Physics, Center for Condensed Matter Sciences, University of Florida.
⊥ Present address: National High Magnetic Field Laboratory, Tallahassee, FL 32310-3706.

(1) Sato, O.; Iyoda, T.; Fujishima, A.; Hashimoto, K. *Science* **1996**, *272*, 704.
(2) Yoshizawa, K.; Mohri, F.; Nuspl, G.; Yamabe, T. *J. Phys. Chem. B* **1998**, *102*, 5432.
(3) Sato, O.; Einaga, Y.; Fujishima, A.; Hashimoto, K. *Inorg. Chem.* **1999**, *38*, 4405.
(4) Bleuzen, A.; Lomenech, C.; Escax, V.; Villain, F.; Varret, F.; Cartier dit Moulin, C.; Verdaguer, M. *J. Am. Chem. Soc.* **2000**, *122*, 6648.
(5) Cartier dit Moulin, C.; Villain, F.; Bleuzen, A.; Arrio, M. A.; Sainctavit, P.; Lomenech, C.; Escax, V.; Baudelet, F.; Dartyge, E.; Gallet, J. J.; Verdaguer, M. *J. Am. Chem. Soc.* **2000**, *122*, 6653.
(6) Pejakovic, D. A.; Manson, J. L.; Miller, J. S.; Epstein, A. J. *Phys. Rev. Lett.* **2000**, *85*, 1994.
(7) Escax, V.; Bleuzen, A.; Cartier dit Moulin, C.; Villiam, F.; Goujon, A.; Varret, F.; Verdaguer, M. *J. Am. Chem. Soc.* **2001**, *123*, 12536.
(8) Kawamoto, T.; Asai, Y.; Abe, S. *Phys. Rev. Lett.* **2001**, *86*, 348.
(9) Shimamoto, N.; Ohkoshi, S.-i.; Sato, O.; Hashimoto, K. *Inorg. Chem.* **2002**, *41*, 678.
(10) Liu, H. W.; Matsuda, K.; Gu, Z. Z.; Takahashi, K.; Cui, A. L.; Nakajima, R.; Fujishima, A.; Sato, O. *Phys. Rev. Lett.* **2003**, *90*, 167403.
(11) Kamiya, M.; Hanawa, M.; Moritomo, Y.; Isobe, Y.; Tateishi, J.; Kato, K.; Nakamura, A. *Phys.Rev. B* **2004**, *69*, 052102.
(12) Boukheddaden, K.; Nishino, M.; Miyashita, S.; Varret, F. *Phys. Rev. B* **2005**, *72*, 014467.
(13) Gawali-Salunke, S.; Varret, F.; Maurin, I.; Enachescu, C.; Malarova, M.; Boukheddaden, K.; Codjovi, E.; Tokoro, H.; Ohkoshi, S.; Hashimoto, K. *J. Phys. Chem. B* **2005**, *109*, 8251.
(14) Cartier dit Moulin, C.; Champion, G.; Cafun, J. D.; Arrio, M. A.; Bleuzen, A. *Angew. Chem., Int. Ed.* **2007**, *46*, 1287.
(15) Culp, J. T.; Park, J.-H.; Benitez, I. O.; Huh, Y.-D.; Meisel, M. W.; Talham, D. R. *Chem. Mater.* **2003**, *15*, 3431.
(16) Culp, J. T.; Park, J.-H.; Meisel, M. W.; Talham, D. R. *Inorg. Chem.* **2003**, *42*, 2842.
(17) Culp, J. T.; Park, J.-H.; Meisel, M. W.; Talham, D. R. *Polyhedron* **2003**, *22*, 3059.
(18) Culp, J. T.; Park, J.-H.; Benitez, I. O.; Meisel, M. W.; Talham, D. R. *Polyhedron* **2003**, *22*, 2125.
(19) Culp, J. T.; Park, J.-H.; Frye, F.; Huh, Y.-D.; Meisel, M. W.; Talham, D. R. *Coord. Chem. Rev.* **2005**, *249*, 2642.
(20) Park, J.-H.; Cizmar, E.; Meisel, M. W.; Huh, Y. D.; Frye, F.; Lane, S.; Talham, D. R. *Appl. Phys. Lett.* **2004**, *85*, 3797.
(21) Park, J.-H.; Huh, Y. D.; Cizmar, E.; Gamble, S. G.; Talham, D. R.; Meisel, M. W. *J. Magn. Magn. Mater.* **2004**, *1116*, 272–276.
(22) Park, J.-H.; Frye, F.; Lane, S.; Cizmar, E.; Huh, Y. D.; Talham, D. R.; Meisel, M. W. *Polyhedron* **2005**, *24*, 2355.
(23) Frye, F. A.; Pajerowski, D. M. B.; Lane, S. M.; Anderson, N. E.; Park, J.-H.; Meisel, M. W.; Talham, D. R. *Polyhedron* **2007**, *26*, 2281.

10.1021/cm800576s CCC: $40.75 
Published on Web 08/07/2008

orientation and decreasing in the other, when the externally applied magnetic field was less than 1.5 kG and the temperature was 5 K for a 160 nm thick film. We previously communicated this finding[20,23] and proposed a qualitative model for the anisotropic behavior that depends on the influence of magnetic moments in the film before photoexcitation. In this paper, we present a complete study of the fabrication and magnetic behavior of thin films of $A_jCo_k[Fe(CN)_6]_l \cdot nH_2O$, including thorough investigations of the parameters that determine the photoinduced magnetic behavior. These observations reveal flaws in the earlier qualitative model for the novel thin film behavior, and our present analysis suggests the source of the anisotropic behavior is the interface between the magnetic thin film and the solid support.

Compounds of the family $A_jCo_k[Fe(CN)_6]_l \cdot nH_2O$ with partial $[Fe(CN)_6]^{3-}$ vacancies have been shown to exhibit CTIST (charge transfer induced spin transition).[9] When this complex is cooled from room temperature to 50 K, there is a charge transfer from the $Co^{II}$ to the $Fe^{III}$ along with a spin-crossover event for the cobalt ion, while the iron remains low spin. Specifically, regions of the compound transition from ferrimagnetic $Co^{II}$ ($S = {}^3/_2$), $Fe^{III}$ ($S = 1/2$) to diamagnetic $Co^{III}$ ($S = 0$), $Fe^{II}$ ($S = 0$), resulting in a decrease in magnetism. However, the transition is not complete. Local inhomogeneities in the distribution of ferricyanide vacancies cause some of the material to remain in the ferrimagnetic state. This component of the material is referred to as nonswitchable pairs, or primordial spins,[20] and undergoes magnetic ordering near 15 K. The $Co^{III}(ls)-Fe^{II}$ pairs of the diamagnetic component may be photoexcited using visible light and converted back to the ferrimagnetic $Co^{II}(hs)-Fe^{III}$ pairs, thereby increasing the magnetization[1,2,4,9,14] and placing the material in a long-lived, metastable state. The process is reversible by thermal treatment, allowing the photoexcited states to relax to the diamagnetic state.[3]

Methods of generating films and coatings of Prussian blue and its analogues include electrochemical methods,[24–30] dip-coating or spin-casting of colloidal solutions,[24,31] and adsorption onto sol−gel films.[32,33] Routes to films with nanoscale thickness include synthesis of cyanometallate monolayers[16,18] and adsorption of the cyanometallate at Langmuir monolayers,[34,35] charged amphiphiles,[36–39] and polyelectrolyte films.[40] One of these methods described by Einaga and co-workers[39] reports anisotropy in a cobalt iron Prussian blue analogue film, although no photoinduced decrease was observed. Films of intermediate, submicrometer thickness can be prepared by synthesizing the cyanometallate directly on surfaces by sequential adsorptions of the constituent ions.[15,19–22,41–43] The sequential adsorption approach affords fine thickness control of homogeneous films on a variety of different solid supports and the ability to easily tailor the chemical composition. Sequential adsorption techniques were used to produce the films described in this study.

## Experimental Section

**Reagents and Materials.** All reagents were purchased from Sigma-Aldrich or Fisher Scientific and used without further purification. Trace metal-grade nitric acid was used for inductively coupled plasma mass spectrometry (ICP-MS) experiments, and all other reagents were ACS grade. Deionized (DI) water (18 MΩ) was used for all experiments. Melinex, a polyethylene terephthalate polymer 535/380 gauge, was obtained from DuPont Teijin films and was used as the solid support for all of the thin films reported herein.

**Sample Preparation of $A_jCo_k[Fe(CN)_6]_l \cdot nH_2O$ thin films.** *$Rb_{0.7}Co_4[Fe(CN)_6]_{3.0} \cdot 6H_2O$.* Slow growth.[43] A sheet of Melinex was placed in a 5 mM aqueous solution of cobalt(II) nitrate for 60 s. The film was rinsed with DI water, then rinsed with methanol and dried with a stream of nitrogen. The film was then placed in a solution containing 20 mM potassium ferricyanide and 0.12 mM rubidium nitrate for 60 s. The film was rinsed with DI water, then rinsed with methanol and dried with a stream of nitrogen to complete one cycle. The process was repeated for 5, 10, 20, 40, or 75 cycles to generate films of varied thickness. Metal content was determined by ICP-MS using a 40 cycle film with resultant metal percentages of Rb 3.2%, Co 12.7%, and Fe 9.0%.

*$Rb_{2.3}Co_4[Fe(CN)_6]_{3.1} \cdot 5.4H_2O$. Slow* growth. The method was similar to the one described above, except a potassium ferricyanide solution containing 12 mM rubidium nitrate was used. The film was rinsed with DI water and methanol then dried. Both 40 and 75 deposition cycle films were generated. Metal content was determined by ICP-MS using a 40 cycle film with resultant metal percentages of Rb 10.6%, Co 12.4%, and Fe 8.9%.

*$K_{0.5}Co_4[Fe(CN)_6]_{3.2} \cdot 4.8H_2O$. Slow* growth. The method was similar to the one described above, except a potassium ferricyanide solution containing 12 mM potassium nitrate was used. Both 40 and 75 deposition cycle films were generated. Metal content was determined by ICP-MS using a 40 cycle film with resultant metal percentages of K 0.37%, Co 4.5%, and Fe 3.4%.

*$Rb_{0.7}Co_4[Fe(CN)_6]_{3.0} \cdot 6H_2O$. Fast* growth.[20] Although a hydrophilic solid support such as silicon has been previously used by

(24) Neff, V. D. *J. Electrochem. Soc.* **1978**, *125*, 886.
(25) Itaya, K.; Ataka, T.; Toshima, S. *J. Am. Chem. Soc.* **1982**, *104*, 4767.
(26) Buschmann, W. E.; Paulson, S. C.; Wynn, C. M.; Girtu, M. A.; Epstein, A. J.; White, H. S.; Miller, J. S. *Chem. Mater.* **1998**, *10*, 1386.
(27) Lundgren, C. A.; Murray, R. W. *Inorg. Chem.* **1988**, *27*, 933.
(28) Ohkoshi, S.-i.; Einaga, Y.; Fujishima, A.; Hashimoto, K. *J. Electroanal. Chem.* **1999**, *473*, 245.
(29) Ivanov, V. D.; Kaplun, M. M.; Kondrat'ev, V. V.; Tikhomirova, A. V.; Zigel′, V. V.; Yakovleva, S. V.; Malev, V. V. *Russ. J. Electrochem.* **2002**, *38*, 173.
(30) deTacconi, N. R.; Rajeshwar, K.; Lezna, R. O. *Chem. Mater.* **2003**, *15*, 3046.
(31) Toshima, N.; Lin, R. J.; Kaneko, M. *Chem. Lett.* **1990**, 485.
(32) Honda, K.; Hayashi, H.; Chiba, K. *Chem. Lett.* **1988**, 191.
(33) Guo, Y.; Guadalupe, A. R.; Resto, O.; Fonseca, L. F.; Weisz, S. Z. *Chem. Mater.* **1999**, *11*, 135.
(34) Torres, G. R.; Agricole, B.; Delhaes, P.; Mingotaud, C. *Chem. Mater.* **2002**, *14*, 4012.
(35) Romualdo-Torres, G.; Agricole, B.; Mingotaud, C.; Ravaine, S.; Delhaes, P. *Langmuir* **2003**, *19*, 4688.
(36) Mingotaud, C.; Lafuente, C.; Amiell, J.; Delhaes, P. *Langmuir* **1999**, *15*, 289.
(37) Yamamoto, T.; Umemura, Y.; Sato, O.; Einaga, Y. *Chem. Mater.* **2004**, *16*, 1195.
(38) Yamamoto, T.; Umemura, Y.; Sato, O.; Einaga, Y. *Chem. Lett.* **2004**, *33*, 500.
(39) Yamamoto, T.; Umemura, Y.; Sato, O.; Einaga, Y. *J. Am. Chem. Soc.* **2005**, *127*, 16065.
(40) Jaiswal, A.; Colins, J.; Agricole, B.; Delhaes, P.; Ravaine, S. *J. Colloid Interface Sci.* **2003**, *261*, 330.
(41) Millward, R. C.; Madden, C. E.; Sutherland, I.; Mortimer, R. J.; Fletcher, S.; Marken, F. *J. Chem. Soc., Chem. Commun.* **2001**, 1994.
(42) Pyrasch, M.; Tieke, B. *Langmuir* **2001**, *17*, 7706.
(43) Jin, W.; Toutianoush, A.; Pyrasch, M.; Schnepf, J.; Gottschalk, H.; Rammensee, W.; Tieke, B. *J. Phys. Chem. B* **2003**, *107*, 12062.

**Scheme 1. Sequential Adsorptions Method Showing the Deposition of Cationic and Anionic Building Blocks to Form the Cobalt Iron Prussian Blue Analogue**

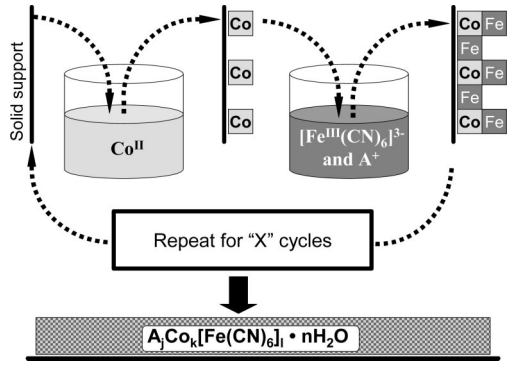


us, for the work reported here, Melinex was used as a solid support. The solid support was quickly immersed 5 times in a 5 mM aqueous solution of cobalt(II) nitrate. The excess solution was drained, and the solid support was quickly immersed 5 times in an aqueous solution of 20 mM potassium ferricyanide and 12 mM rubidium nitrate. The solid support was then rinsed with DI water. This process was repeated 1, 5, 10, 20 or 40 times to generate films of increasing thickness. After deposition, the film was rinsed with methanol and dried under a vacuum. Metal content was determined by ICP-MS using a 40 cycle film with resultant metal percentages of Rb 3.2%, Co 12.7%, and Fe 9.0%.

**Instrumentation.** The elemental analyses were performed by ICP-MS on a Thermo-Finnigan Element-2 spectrometer. FT-IR spectra were recorded using a Bruker Vector 22 spectrometer. Atomic force microscopy (AFM) measurements were performed using a Digital Instruments multimode scanning probe microscope. Scanning electron microscopy (SEM) images were obtained using a Hitachi S-4000 FE-SEM. Magnetic measurements were made using a Quantum Design MPMS XL superconducting quantum interference device (SQUID) magnetometer. A bundle of 10 optical fibers, 270 $\mu$m O.D. (Ocean Optics model 200-UV), was used to introduce light, from a room-temperature halogen-light source, of 1−2 mW power (∼400−1100 nm) into the SQUID magnetometer for photoinduced experiments.[44] Irradiation at low temperatures does cause a small amount of heating of the specimens, less than a few tenths of a Kelvin, as evidenced by detectable glitches in the magnetic response when the light is turned on or off, so corrections of the magnetic data are not necessary.

**Analysis Preparations.** Melinex supports were cut to 8 cm × 2.5 cm and cleaned using methanol and used for all processes. ICP-MS samples of 40 cycle films were prepared by digesting the thin film and Melinex in 2 mL of boiling, concentrated sulfuric acid for 4 h, resulting in a black liquid. Concentrated nitric acid (0.5 mL) was then added dropwise, before diluting the mixture to 100 mL with DI water. The samples were compared to matrix matched metal blends between 1 ppm and 1 ppb. The resultant concentrations were normalized to a unit cell formula $A_jCo_4[Fe(CN)_6]_l \cdot nH_2O$ by fixing 4 cobalt ions per unit cell. The unit cell formula was used as the molar mass for subsequent calculations. The water content is assumed to be water molecules coordinated to the cobalt and was determined by the number of ferricyanide vacancies, specifically, $n = 6(4 - l)$. Using AFM, we obtained thickness and roughness data by averaging the measurements of five different 4 $\mu$m$^2$ scans. Thickness was determined by investigating the height difference between the average thickness of the film and the solid support. The root mean squared (rms) average of height deviations taken from the mean data plane is used to express roughness. For magnetic measurements the samples were cut into squares (∼10.5 mm$^2$) and stacked, with the surfaces parallel, into a polyethylene sample holder. Background contributions of the container and Melinex were measured separately and subtracted from the raw data.

(44) Park, J.-H. Ph.D. Thesis, University of Florida, Gainesville, FL, 2006.

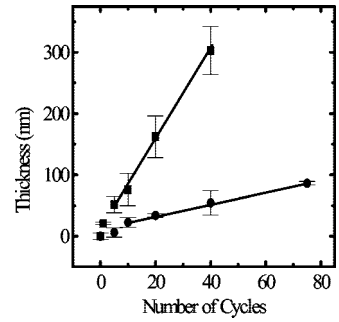


**Figure 1.** Thickness vs number of cycles for the "slow" growth (●) and "fast" growth (■) sequential adsorption deposition methods used to generate thin films of the cobalt iron Prussian blue analogue. Uncertainty bars represent the average thickness standard deviation. Lines are drawn to guide the eyes and show the linear film growth with deposition cycles once a continuous film is established.

## Results

**Film Generation and Characterization.** All films were generated by sequentially adsorbing $Co^{2+}$ and $Fe(CN)_6^{3-}$ from aqueous solution, adapting procedures previously described by our group[15,18–23] and others[41–43] for Prussian blue films and other Prussian blue analogues (Scheme 1). The thickness can be tuned by adjusting the number of deposition cycles, and films can be fabricated over large surface areas using a variety of solid supports. This last point becomes important because transparent, diamagnetic solid supports are needed for photomagnetic experiments

Deposition normally begins by adsorption of ions to a charged surface. For the Melinex supports, the surface charge results from a nitrogen-containing, adhesion-promoting coating placed on the surface by the manufacturer. It takes several deposition cycles to achieve complete surface coverage. Our group previously demonstrated that homogeneous surface coverage can be achieved for a thin film by first modifying the surface with a cyanometallate monolayer, prepared using Langmuir−Blodgett methods.[15,18,21] However, the studies described in the present paper utilize a wider range of thicknesses (50−300 nm), and the template layer was not employed.

During a deposition cycle, the solid support was first immersed in an aqueous solution containing $Co^{2+}$ ions, followed by immersion in a solution containing $A^+$ and $[Fe(CN)_6]^{3-}$ ions. The process can be controlled to alter the rate of deposition, and two methods, referred to here as "slow" and "fast", were used to generate films. In the "slow" method, the substrate is rinsed between changing solutions, limiting the amount of material deposited during each cycle. For the "fast" method, substrates were immersed in both solutions before rinsing, resulting in a film that developed quickly. Film thickness, measured using AFM, increases with number of cycles for both methods (Figure 1).

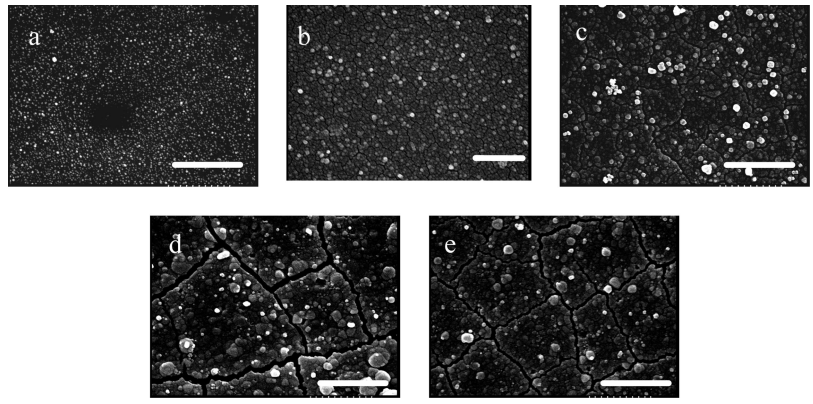


**Figure 2.** (a−e) SEM images of "fast" method films, with thicknesses of 21, 51, 75, 160, and 300 nm, respectively. A 1 $\mu$m scale bar is shown in each image. The deposition method develops a continuous film after 5 cycles (b). The surface morphology is retained as the film develops beyond 5 cycles.

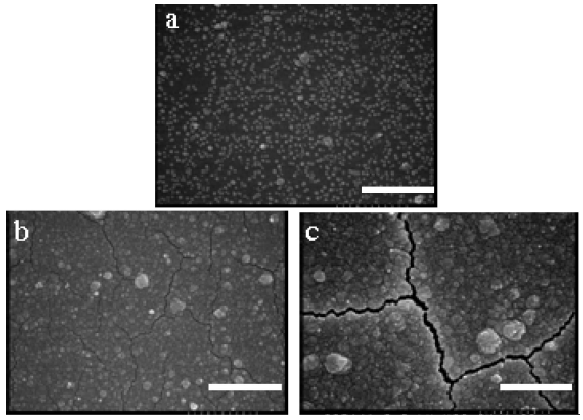


**Figure 3.** (a−c) SEM images of "slow" films, with thicknesses 22, 34, and 71 nm, respectively. A 1 $\mu$m scale bar is shown in each image. Continuous coverage is achieved after 20 cycles (b); less material is deposited by the "slow" method when compared to the "fast" method. "Slow" films show roughness and surface coverage similar to "fast" films of similar thicknesses.

The surface topology of the films can be compared with SEM, Figures 2 and 3. After only one cycle of the "fast" method, the substrate is still visible, indicating that contiguous coverage is not yet achieved. It takes five cycles to completely cover the substrate with powderlike features. The surface morphology is retained as the film develops beyond 5 cycles (Figure 2). Using the "slow" method, complete coverage is not obtained until 20 cycles, at which point the films show similar morphology to those of comparable thickness generated with the "fast" method. Complete surface coverage is achieved between 30 and 50 nm of thickness for both methods. Surface roughness measurements confirm the SEM observations (Table 1).

All films are light pink, with uniform coloration over the surface of the substrate. The room-temperature FT-IR ATR spectrum shown in Figure 4 for a 160 nm film was obtained by pressing the sample against a silicon ATR crystal. The spectrum displays three cyanide stretching bands, a sharp peak at 2169 $cm^{-1}$, attributed to cyanide bridging $Co^{II}$(hs)−$Fe^{III}$, a broader peak centered at 2110 $cm^{-1}$, assigned to cyanide bridging $Co^{III}$(ls)−$Fe^{II}$, and a shoulder at 2085 $cm^{-1}$ due to cyanide bridging $Co^{II}$(hs)−$Fe^{II}$. The energies of these stretches agree with previously reported data[3] for powdered solids of similar rubidium concentrations, confirming that the targeted material is deposited on the surface.

**Table 1. AFM Thickness and Roughness Data for Films of $Rb_{0.7}Co_4[Fe(CN)_6]_{3.0} \cdot 6H_2O$**

| no. of cycles | average thickness (nm) | rms roughness[a] (nm) |
|---|---|---|
| | "slow" method | |
| 20 | 34 ± 3 | 12 |
| 40 | 71 ± 15 | 22 |
| 75 | 86 ± 3 | 37 |
| | "fast" method | |
| 5 | 51 ± 8 | 17 |
| 10 | 75 ± 20 | 23 |
| 20 | 160 ± 30 | 62 |
| 40 | 300 ± 30 | 100 |

[a] rms = Average of height deviations taken from the mean thickness plane.

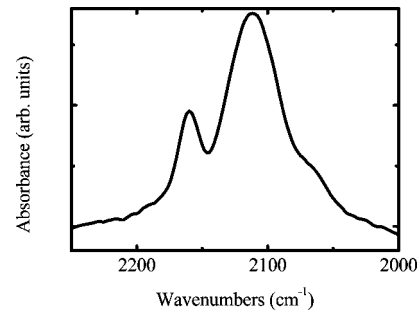


**Figure 4.** Room-temperature FT-IR ATR spectrum of a 160 nm $Rb_{0.7}Co_4[Fe(CN)_6]_{3.0} \cdot 6H_2O$ film on Melinex. The sharp peak at 2169 $cm^{-1}$ is attributed to the $Co^{II}$(hs)-NC-$Fe^{III}$ bridging cyanide stretch and the broad peak centered at 2110 $cm^{-1}$ is assigned to $Co^{III}$(ls)−NC−$Fe^{II}$. The shoulder at 2085 $cm^{-1}$ is due to cyanide bridging $Co^{II}$(hs)−NC−$Fe^{II}$.

**Magnetic Behavior with $H_E$ Parallel to the Thin Films.** The thin films exhibit magnetic behavior similar to powder samples, when oriented parallel to the external magnetic field, $H_E$. Temperature-dependent zero-field-cooled (zfc) and field-cooled (fc) measurements from 5 to 30 K were performed with the film plane parallel to $H_E = 200$ G, and data from a 160 nm film are shown in Figure 5. An apparent $T_C$, defined here as the temperature at which the magnetization begins to increase, is near 15 K. The fc and zfc magnetizations bifurcate near 9 K, and there is a maximum in zfc magnetization at $T \approx 7$ K. Upon photoexcitation, $T_C$ increases to 18 K, the bifurcation of zfc and fc data increases to 11 K, and the peak temperature in zfc magnetization shifts to $T \approx 9.5$ K. (Figure 5)

The magnetic response is consistent with the reported behavior of powder samples of cobalt iron Prussian blue

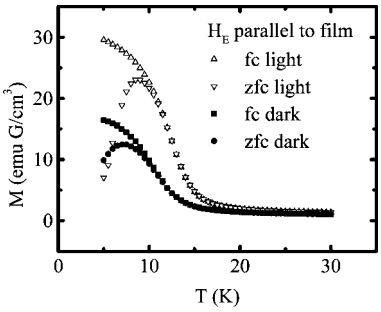


**Figure 5.** Plots of fc and zfc DC magnetization of a 160 nm thick film of $Rb_{0.7}Co_4[Fe(CN)_6]_{3.0}\cdot 6H_2O$ parallel to $H_E = 200$ G in dark and photoinduced (light) states.

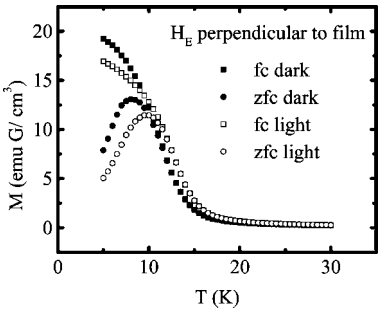


**Figure 6.** Plots of fc and zfc DC magnetization of a 160 nm thick film of $Rb_{0.7}Co_4[Fe(CN)_6]_{3.0}6H_2O$ perpendicular to $H_E = 200$ G in dark and photoinduced (light) states.

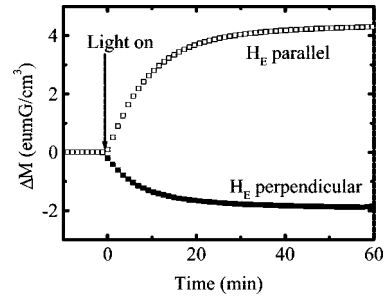


**Figure 7.** Anisotropy in the photoinduced magnetization of a 75 nm film of $Rb_{0.7}Co_4[Fe(CN)_6]_{3.0}\cdot 6H_2O$, measured at 5 K with the measuring field of 200 G oriented parallel and perpendicular to the film. The time axis is relative to the instant the light is applied and $\Delta M = M(t) - M(t = 0)$.

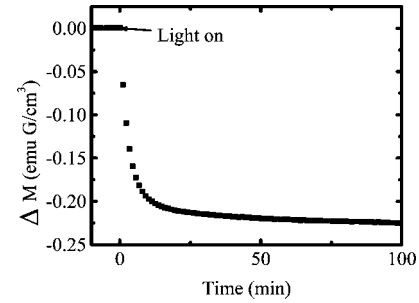


**Figure 8.** Change in magnetization for a 86 nm film of $K_{0.5}Co_4[Fe(CN)_6]_{3.2}\cdot 4.8H_2O$ perpendicular to $H_E$ of 200 G at 5 K. A photoinduced decrease in magnetization is observed. The axes are as defined in Figure 7.

analogues.[3,4,39] The dark state response is attributed to glassy behavior[6,45] of disordered interacting clusters of ferrimagnetically ordered $Co^{II}(hs)-Fe^{III}$ regions that have not undergone charge transfer and spin-crossover demagnetization upon cooling. With illumination, some diamagnetic pairs that experienced spin-crossover upon cooling are switched to the $Co^{II}(hs)-Fe^{III}$ state, causing an increase of the concentration and size of ferrimagnetic clusters. The result is enhanced magnetization, and an increase in blocking temperature, defined as the temperature at which the fc and zfc plots bifurcate, from 9 to 11 K because of larger size or increased concentration of domains.[6,45]

**Anisotropic Photomagnetic Behavior.** With the films oriented perpendicular to the applied magnetic field, the photoeffects are different. The temperature dependent fc and zfc measurements from 5 to 30 K of the same 160 nm film as shown in Figure 5, for $H_E = 200$ G perpendicular to the film, are shown in Figure 6 for both the light and dark states. The dark state data are essentially the same as in the parallel orientation, and subtle differences may suggest the film is somewhat better ordered perpendicular to the surface than parallel to it. In addition, upon photoexcitation, the $T_C$ of 16 K increases to 18 K, and there is also an increase in the blocking temperature shifting from 10 to 11 K. These trends are similar to the ones observed for $H_E$ parallel to the film. However, the magnetization of the photoinduced (light) sample is now lower than the dark sample, i.e., there is a photoinduced decrease in magnetization below nominally 10 K.

The anisotropic photoinduced response of the thin films is more clearly illustrated by plotting the time dependent change of the magnetization upon irradiation with visible light. Figure 7 shows the magnetization versus time at 5 K, with $H_E = 200$ G in both orientations, for a 75 nm thick film. Upon irradiation, the magnetization of the film increases when oriented parallel to $H_E = 200$ G, and decreases when perpendicular to the same $H_E$.

**Alkali Cation Dependence.** Photoinduced magnetism in the cobalt iron Prussian blue is not restricted to $Rb^+$ analogues, but has also been reported in $Na^+$, $K^+$, and $Cs^+$ salts.[1–4,7,9,28] Other thin film compositions were therefore investigated to determine if the anisotropy seen for the $Rb^+$ analogues depends on chemical formula. A potassium containing film with formula $K_{0.5}Co_4[Fe(CN)_6]_{3.2}\cdot 4.8H_2O$ was generated. The time dependent change in magnetization of an 86 nm film at 5 K is shown in Figure 8 when $H_E = 200$ G and is perpendicular to the film. As for the $Rb^+$ films, a photoinduced decrease in magnetization was observed, indicating that the anisotropic photoresponse is not alkali cation specific.

Increasing the concentration of alkali ions in the interstitial sites of powdered solids of cobalt iron Prussian blue analogues leads to fewer ferricyanide vacancies and increases the average ligand field strength around the cobalt.[4,5,9] The increased ligand field strength inhibits the temperature dependent spin crossover, eliminating the presence of photoswitchable pairs and, therefore, any photoinduced change in magnetism. The influence of the alkali cation content in the films was compared by measuring the time dependent photoinduced magnetization of slow-growth 75 cycle films (86 nm) of $Rb_{0.7}Co_4[Fe(CN)_6]_{3.0}\cdot 6H_2O$ and $Rb_{2.3}Co_4[Fe-$

(45) Mydosh, J. A. *Spin Glasses*; Taylor and Francis: Washington, D.C., 1993.

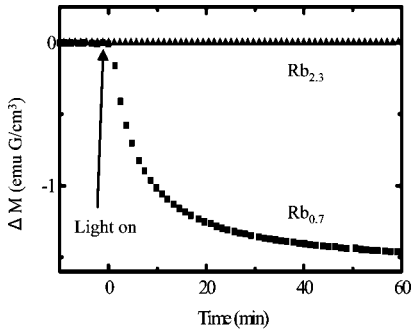


**Figure 9.** Rubidium ion concentration dependence of the photoinduced magnetization of cobalt iron Prussian blue analogue films, (▲) $Rb_{2.3}Co_4[Fe(CN)_6]_{3.1}\cdot 5.4H_2O$, and (■) $Rb_{0.7}Co_4[Fe(CN)_6]_{3.0}\cdot 6H_2O$ (slow growth 75 cycles, 86 nm) measured at 5 K with $H_E = 200$ G applied perpendicular to the planes of the films. Films with higher rubidium concentration do not experience a photoinduced decrease in magnetism. Axes are as defined in Figure 7.

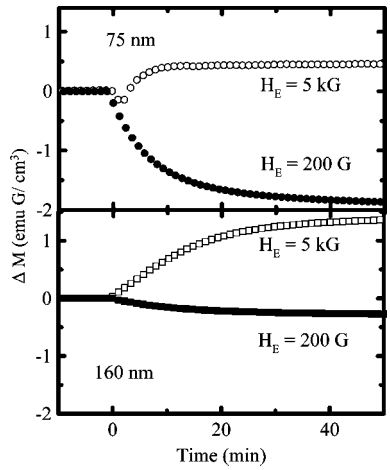


**Figure 10.** Photoinduced magnetization of $Rb_{0.7}Co_4[Fe(CN)_6]_{3.0}\cdot 6H_2O$ measured at 5 K for different values of $H_E$ applied perpendicular to the plane of the film. Top, a 75 nm film with $H_E = 200$ G (●) and 5 kG (○), and bottom, a 160 nm film with $H_E = 200$ G (■) and 5 kG (□). The axes are as defined in Figure 7.

$(CN)_6]_{3.1}\cdot 5.4H_2O$ (Figure 9). Consistent with the behavior of powdered solids, there is no photoinduced change in magnetization for thin films with higher alkali ion content.

**Field-Dependent Magnetic Behavior of 75 and 160 nm Films.** The effect of the external magnetic field strength on the photoinduced decrease in magnetism was explored by comparing the time dependent change in magnetization in external fields of $H_E = 200$ G and 5 kG. Data for 75 and 160 nm films oriented perpendicular to $H_E$ are presented in Figure 10. Whereas the films show a photoinduced decrease of magnetization for $H_E = 200$ G, both samples show a photoinduced increase in magnetization when $H_E$ is increased to 5 kG.

The observation that the increase or decrease of photoinduced magnetization is related to the strength of $H_E$ suggests that there should be a field for which no photoinduced change in magnetism is observed. To look for this transition, we measured the field-dependent magnetization of a 160 nm film at 5 K for both the dark state and the light state (Figure 11). When the $H_E$ is around 1.5 kG, the photoinduced magnetization becomes greater relative to the dark state magnetization, so a photoinduced increase in magnetization is expected for

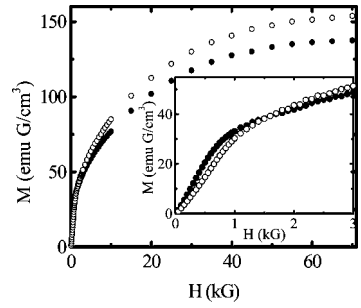


**Figure 11.** Field-dependent magnetization of a 160 nm film of $Rb_{0.7}Co_4[Fe(CN)_6]_{3.0}\cdot 6H_2O$ measured at 5 K with the magnetic field perpendicular to the film. At a $H_E \approx 1.5$ kG, no difference in magnetization is observed between the dark state (•) and the photoinduced state (○). The inset expands the low-field region.

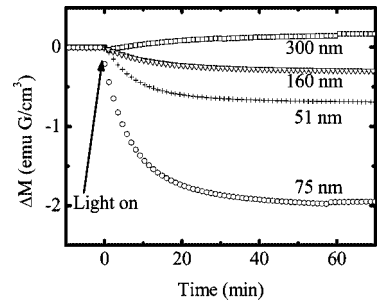


**Figure 12.** Thickness dependence of the photoinduced magnetization in cobalt iron Prussian blue analogue thin films $Rb_{0.7}Co_4[Fe(CN)_6]_{3.0}\cdot 6H_2O$ at 5 K with $H_E = 200$ G perpendicular to the film plane. The films less than 160 nm thick show a decrease in magnetization upon illumination. As films become thicker, the photoinduced effect becomes an increase in magnetization, similar to that of bulk powder samples. Axes are as defined in Figure 7.

fields greater than 1.5 kG. Below 1.5 kG, the magnetization of the photoinduced state is less than the dark state, so a photoinduced decrease in magnetization is observed.

**Effect of Film Thickness.** The photoinduced decrease in magnetism is not observed for powdered solids, only in continuous thin films, so the influence of film thickness was investigated by taking advantage of the ability to control the thickness of the films with the sequential adsorption process. The photomagnetic response of four films, with thicknesses of 51, 75, 160, and 300 nm, were measured at 5 K with $H_E = 200$ G applied perpendicular to the plane of the films, Figure 12. The 51, 75, and 160 nm films all show a photoinduced decrease. However, for the 300 nm film, a photoinduced increase in magnetization is observed. In addition, the magnitude of the effect varies as the thickness changes. At first, the magnitude of the decrease becomes larger as films become thicker. However, by the time the film is 160 nm thick, the magnitude of the photoinduced decrease has diminished. By 300 nm, the effect is reversed, and a photoinduced increase is observed.

**Temperature Dependence of the Anisotropy.** Magnetic data in Figures 7–12 were obtained at 5 K, below the onset of ferrimagnetic ordering of the magnetic domains. Above the ordering temperature, photoswitchable pairs are still present because the charge transfer/spin-crossover state persists until much higher temperatures, nominally up to 100 K. In an attempt to determine if the photoinduced decrease is a property of the ordered state, the photoresponse was studied above the ordering temperature of a film that

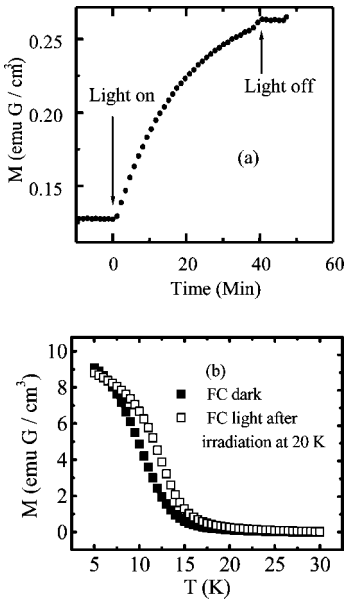


**Figure 13.** (a) Photoinduced magnetism of a 160 nm film of $Rb_{0.7}Co_4[Fe(CN)_6]_{3.0}\cdot 6H_2O$ at 20 K with $H_E = 200$ G perpendicular to the film. The light is applied at $t = 0$ min and discontinued at $t = 40$ min. The data show that at 20 K, above the onset of ferrimagnetic ordering, there is a photoinduced increase in magnetism. Thermal effects associated with light turn-off can be seen near 40 min. (b) The FC dark (i.e., before any irradiation) and FC light, after 40 min of irradiation at 20 K, are shown for $H_E = 200$ G perpendicular to the film.

was previously shown to exhibit a photoinduced decrease at 5 K. The time-dependent response of the 160 nm film studied in Figure 12 was measured at 20 K (Figure 13a). Above the ordering temperature, the 160 nm film displays a photoinduced increase in magnetism, which might be interpreted as evidence that the photoinduced decrease is a property of the film below the ordering temperature. However, motivated by the results of Figure 6, where the decrease of the magnetization is only maintained below about 10 K when $H_E = 200$ G, the film was FC to 5 K after 40 min of irradiation at 20 K and measured in a field of 200 G (Figure 13b). The striking result is that the decrease in the magnetization was observed, albeit below about 7 K.

## Discussion

Cobalt iron Prussian blue analogue films prepared using sequential adsorption methods exhibit several properties typical of the more extensively studied powdered solids. With appropriate composition, a fraction of the material in the films undergoes charge transfer and spin-crossover and the remaining high spin fraction orders giving a ferrimagnetic state at low temperature. The low-temperature magnetic properties are consistent with cluster spin glass behavior, which also characterizes the known powdered solids.[6] Upon photoexcitation, $T_C$ increases, as does the blocking temperature, indications that the size or concentration of magnetic domains in the sample increases. With the film oriented parallel to the magnetic field, photoexcitation yields an increase in magnetization. Compositions that exhibit these photoeffects in powdered solids also show them in thin films. These observations indicate that the microscopic mechanism by which the magnetization changes with light is the same in the films as was seen previously with the powdered solids. However, the photoresponse of the films is anisotropic. The photoinduced increase in magnetism seen when the film is oriented parallel to the magnetic field becomes a photoinduced decrease below ~10 K, when the film is oriented perpendicular to $H_E = 200$ G. An orientation-dependent photoinduced decrease has not been seen in the powdered solids.

The anisotropic photoeffects are influenced by a number of factors. The first is the external magnetic field strength; by increasing $H_E$ to ~1.5 kG, with $H_E$ perpendicular to the film, the photoinduced decrease in magnetization becomes a photoinduced increase at 5 K. Film thickness also plays an important role. As films become thicker, the photoinduced decrease diminishes and, by 300 nm, becomes a photoinduced increase, at 5 K, like in the parallel orientation and the analogous powdered solids. Furthermore, the photoinduced decrease is only observed below the ferrimagnetic ordering temperature, and then, only for $T < 10$ K when $H_E = 200$ G. At 20 K, a photoinduced increase is observed, but when subsequently FC in 200 G, a photoinduced decrease is detected below 7 K. Taken together, these observations suggest the photoinduced decrease in magnetization involves a competition between the underlying anisotropy and the externally applied magnetic field, yielding a frustrated state that can be relaxed at sufficiently high temperatures and/or magnetic fields. In addition, thin film organization is a crucial component for observing the effect.

In earlier work, the behavior in the thin films was qualitatively modeled by considering the influence of the dipolar field ($H_D$) emanating from magnetic domains present in the dark state film.[20] Within this model, the photoswitchable components of the films, consisting of diamagnetic $Co^{III}(ls)-Fe^{II}$ pairs that underwent charge transfer and spin-crossover upon cooling, are thought to be located at the edge of magnetic domains, comprising high-spin material that experiences ferrimagnetic ordering at low temperature. With respect to photoinduced effects, these domains can be considered primordial moments, which are estimated to be physically too small and magnetically too weak to be resolved by presently available magnetic imaging techniques. With an applied field perpendicular to the film, these primordial moments will align along $H_E$. The primordial moments will generate a magnetic field that will oppose $H_E$ in the plane of the film. Therefore, the proximal photoinducible regions in the plane of the film will experience both $H_E$ and an opposing $H_D$. The model suggests that when $H_E$ is small, the photoswitchable pairs generate moments that align with $H_D$ against $H_E$, thereby generating a photoinduced decrease in magnetization.

The proposed mechanism is consistent with some of the observations made upon changing different experimental parameters. However, this dipolar field model fails to provide an adequate description of the observed temperature-field dependences (Figures 6, 11, and 13b). Furthermore, when the model is used to generate semiquantitative estimates of the dipolar fields arising from the primordial field regions, the resulting values are considered to be about an order of magnitude too small to explain the results

shown in Figure 11. More likely, the thin film behavior results from a more general effective anisotropy field that may be induced at the interface with the solid support.

Einaga and co-workers[39] reported anisotropic behavior in composite films of the cobalt iron Prussian blue analogue with exfoliated clay and didodecyldimethylammonium bromide. Although the magnetic behavior was anisotropic, no photoinduced decrease was reported. The cobalt iron layers were clearly isolated in the *z*-direction by the smectite clay and didodecyldimethylammonium bromide used to form the film. The in-plane structure was composed of a disordered arrangement of wire or rodlike structures 4 Å thick that give rise to a magnetic easy axis in the film and generate the observed magnetic anisotropy. The intrinsic disorder of the clay-based films causes a decrease in the influence of the anisotropy arising from the interface between the rodlike microstructures and the solid support. This arrangement is significantly different from our system, which is continuous in three-dimensions. The anisotropy in our system is indeed a result of the interface between the magnetic thin film and the solid support.

## Conclusions

Cobalt iron Prussian blue analogue films prepared using sequential adsorption methods exhibit several properties typical of the more extensively studied powdered solids. These observations indicate that the microscopic mechanism by which the magnetization changes with light is the same in the films as for the powdered solids. However, unlike previously studied bulk solids, the photoresponse of the films is anisotropic. The photoinduced increase in magnetism seen when the film is oriented parallel to the magnetic field can become a photoinduced decrease when the film is oriented perpendicular to the magnetic field.

The anisotropic photoeffects are influenced by field strength and its orientation with respect to the interface between the film and the solid support, film thickness, and temperature. The ability to direct a photoinduced magnetic increase or decrease affords another level of control only available in thin films of the cobalt iron Prussian blue analogue and may be useful in potential device applications of this material.

**Acknowledgment.** We acknowledge early contributions from N. E. Anderson, S. M. Lane, and Y.-D. Hu. This work was supported, in part, by NSF DMR-0305371 and DMR-0701400 (M.W.M.) and NSF DMR-0543362 (D.R.T.). SEM images were obtained at the University of Florida electron microscopy core laboratory. ICP-MS data were collected at the Department of Geology, University of Florida.

CM800576S